Journal of Thermal Science Vol.29, No.1 (2020) 182−193

https://doi.org/10.1007/s11630-019-1107-7 **Article ID: 1003-2169(2020)01-0182-12**

Heat Transfer and Thermal Characteristics Effects on Moving Plate Impinging from Cu-Water Nanofluid Jet

DATTA Abanti*, KUMAR Sonal, HALDER Pabitra

Department of Aerospace Engineering and Applied Mechanics, Indian Institute of Engineering Science and Technology, Shibpur, Howrah, West Bengal 711103, India

Abstract: The present article is focused on modelling of flow and heat transfer behaviour of Cu-water nanofluid in a confined slot jet impingement on hot moving plate. Different parameters such as various moving plate velocities, nanoparticles at various concentrations, variation in turbulent Reynolds number and jet nozzle to plate distance have been considered to study the flow field and convective heat transfer performance of the system. Results of distribution of local and average Nusselt number and skin friction coefficients at the plate surface are shown to elucidate the heat transfer and fluid flow process. Qualitative analysis of both stream function and isotherm contours are carried out to perceive the flow pattern and heat transfer mechanism due to moving plate. The results revealed that average Nusselt number significantly rises with plate velocity in addition with jet inlet Reynolds number. Correlations of the average Nusselt numbers are presented.

Keywords: **Cu-water nanofluid, multiphase, mixture model, moving plate, jet impingement, CFD**

1. Introduction

Jet impingement cooling is relatively simple to implement in situations where soaring heat load is to be removed and also a minimum temperature has to be maintained in the system. Another advantage of using jet impingement is that the jet flow defines its own flow path, thus channeling is not required for cooling purpose. Also, jet impingement cooling has potential to remove high heat fluxes if the velocities are such as to produce a high stagnation pressure. Since impinging jets can eliminate heat and mass in reasonably low pressure drop, hence these jets have numerous significant technological applications in many practical areas such as combustor components and gas turbine cooling, electronic cooling, glass sheet tempering, metal plate annealing and medical processing (i.e. freezing of tissues). Nanofluids jets are quite new in research field as coolant. Choi [1] first gave the idea of nanofluids and then Masuda et al. [2] restated the same phenomena. The phenomena are to diffuse nano-sized particles in a base fluid to improve thermal conductivity and heat transfer performance and resulting final form is called “nanofluid”. Nanofluids have enhanced heat transfer performance better than any conventional fluid due to the presence of nanoparticles which poses higher thermal conductivity as compared to liquids. Since long back, researchers have tried to develop new coolant over traditional one to overcome limitation of heat transfer. They have attempted to create new coolants by dispersing small metallic particles in conventional fluids. As compared to gas and liquid particles, solid particles pose greater thermal conductivity.

Received: Nov 6, 2018
Corresponding author: DATTA Abanti E-mail: abanti.datta@gmail.com
Associate editor: MING Tingzhen

Nomenclature

C_P	specific heat	V_P	velocity of moving plate
C_f	skin friction coefficient	W	width of slot jet
f_{drag}	drag function	**Greek letters**	
H	distance between slot and heated plate	ε	dissipation rate of k
k	turbulent kinetic energy	φ	volume concentration of nanoparticles
L	length of the plate	λ	thermal conductivity
N_u	Nusselt number	μ	dynamic viscosity
P	pressure	μ_t	turbulent eddy viscosity
Pr	Prandtl number	ω	specific dissipation rate of k
R_e	Reynolds number	ρ	density
T_H	temperature of heated plate	**Subscripts**	
T_J	inlet temperature of jet	f	base fluid
U	inlet velocity of jet	m	mixture
u	mean component of velocity	nf	nanofluid
u'	fluctuating component of velocity	s	phase

Therefore, coolants with suspended metal particles exhibit enhanced heat removal capabilities, even when very less amount of particles are suspended in the coolants.

Heat and mass transfer performance of circular or radial jet impingement structure have been investigated very vastly. Although, slot jet impingement structures are not that widely used though it has more favourable qualities in comparison to radial jet. Kilic et al. [3,4] have proved experimentally as well as numerically that rectangular channel jets have more control ability due to their simple construction and even have greater uniformity and higher cooling effectiveness. Shariff and Banerjee [5] studied using confined slot-jet impingement on a moving surface.

After Choi [1], researchers have studied on impingement jet cooling using nanofluids. They have used different types of nanoparticles to suspend in base liquid. Roy et al. [6] investigated for radial jet on laminar flow at a Reynolds number of 1200, using water - Al_2O_3 nanofluid to study on thermal fields as well as hydrodynamic fields of cooling system. They have found out that convective heat transfer coefficient is increased by 200% on adding 10% Al_2O_3 nanoparticles in base fluid. Manca et al. [7] numerically simulated on slot jet impinging technique using water - Al_2O_3 nanofluid. They have studied on turbulent flow and effect of different Reynolds numbers on heat transfer characteristics of nanofluid using single phase model. Killic et al. [8] numerically analysed on combined effect of nanofluids and multiple jet impinging technique. It is established by Xuan and Li [9] that only 5% volumetric concentration of Cu nanoparticles can increase heat removal rate by 45% as compared to pure water. Xuan and Li [9] and Li and Xuan [10] have studied suspension of Cu nanoparticles in pure water and they found out that heat transfer is enhanced by 60% when using 2% volumetric concentration of Cu nanoparticles as compared to pure water at the same Reynolds number. Wen and Ding [11] have investigated on Al_2O_3 nanoparticles with pure water and also agreed that using 1.6% volumetric concentration of Al_2O_3 nanoparticles, the local heat transfer coefficient increased about 41% to 47% with contrast to pure water. Rashidi et al. [12] investigated on single slope solar still with nanofluid to obtain entropy generation. Ellahi et al. [13] investigated on MHD (magnetohydrodynamics) Poiseuille flow using kerosene Al_2O_3. Akbarzadeh et al. [14] simulated on corrugated plate with two phase nanofluid and obtained impact of heat transfer characteristics. Shirvan et al. [15] showed heat transfer effect on wavy surface using nanofluid. Ellahi et al. [16] exemplified on rotating disk using nano-ferroliquid. Rajendran [17] experimented on paprabolic dish using SiC water nanofluid.

Scope of this work can be found in industrial applications such as annealing, quenching or cooling of metal plates after hot rolling. As the authors' knowledge, any work including harnessing of improved thermal characteristics of nanofluid in a jet impingement which is further being impinged to cool a heated surface is scarcely reported. Based on the insights garnered from the available literature, slot jet impingement problem with isothermal condition has been numerically studied with addition of normalized plate velocity varying from 0 to 1, jet inlet Reynolds number ($15\,000 < Re < 30\,000$), nanoparticles volume concentration of 0%, 3% and 5%, and normalized distance of separation between the nozzle and the impinged plate H/W ratio 6 and 8, have been

considered to study the flow field and convective heat transfer performance of the system.

2. Mathematical Modeling

2.1 Geometrical configuration

A two-dimensional rectangular flow domain, as shown in Fig. 1(a) which states jet impingement on a hot isothermal moving plate using Cu-water nanofluid, is numerically investigated to assess thermal and fluid-dynamic performance and interpret velocity and temperature fields due to moving plate. The non-uniform grid is arranged with grid adoption y+=1 at viscous sublayer (for k-ω SST model). To obtain the grid independent studies, four different grid distributions are conducted on H/W= 8, V_P = 1 at Re = 30 000. The grid distributions are 300×100, 280×90, 260×80 and 240×70 as shown in Fig. 1(b). Since there is no substantial variation in Nusselt number distribution at 300×100, further simulations are carried out with this grid distribution.

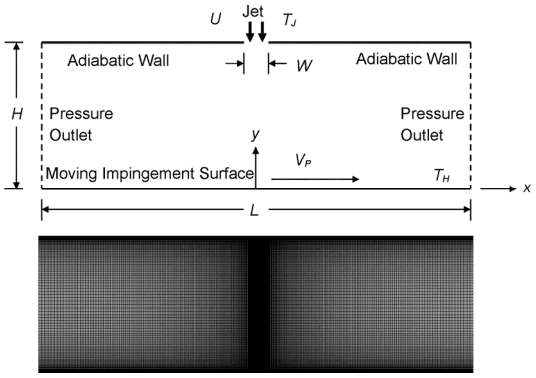

Fig. 1(a) Schematic of the geometrical configuration and stretched mesh layout

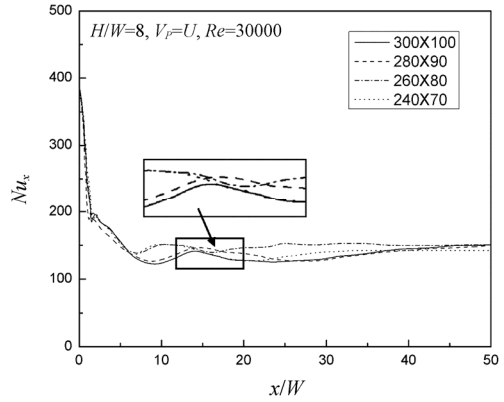

Fig. 1(b) Analysis of gird independence on Nusselt number distribution

The length of the moving plate is L at the bottom which is separated from an upper parallel adiabatic wall by a distance H. The slot-jet of width W is located at the center of the top surface. The right and the left boundaries have been treated as outlets for the flowing fluid. The two-dimensional model has normalized length (L/W) equal to 100 (ranging from –50 to 50) and the normalized height (H/W) which has two values of 6 and 8. The jet slot width W is 6.2 mm. The normalized velocity V_P of the impingement plate (normalized by the jet inlet velocity, U) having a rightward direction, is varied at different values of 0, 0.1, 0.5, 0.75 and 1 where V_P = 0 indicates stationary impingement plate.

2.2 Thermo-physical properties of nanofluid

In the present study, the working fluid is a mixture of water as base fluid and Cu nanoparticles with diameter 20 nm. The volume concentration of Cu nanoparticles in water is taken at 0%, 3% and 5%. The physical properties of water and copper are given in Table 1. Mixing theory is exercised to evaluate the density of nanofluid as:

$$\rho_{nf} = (1-\varphi)\rho_f + \varphi\rho_p \tag{1}$$

The specific heat capacity of Cu-water nanofluid is calculated as:

$$(\rho C_P)_{nf} = (1-\varphi)(\rho C_P)_f + \varphi(\rho C_P)_p \tag{2}$$

The effective dynamic viscosity of the Cu–water nanofluid is computed from Brinkman model [18]:

$$\mu_{nf} = \frac{1}{(1-\varphi)^{2.5}}\mu_f \tag{3}$$

Table 1 Physical properties of water and Cu

Material	ρ/kg·m^{-3}	C_P/J·kg^{-1}·K^{-1}	μ/Pa·s	λ/W·m^{-1}·K^{-1}
Water	998.2	4182	0.001 003	0.6
Cu	8940	385	-	390

2.3 Governing equations

The mixture model [19,20] is utilized for the simulation of multiphase flows where mixing phases may be moving with different velocities or having same velocities with a very strong coupling among them. It is assumed that both phases move at the same velocity. In mixture model approach, continuity, energy and momentum equations are solved for the mixture while volume concentration equation is solved for the secondary phase. Additionally, volume fraction of particles is calculated from the continuity equation of each discrete phase.

$$\frac{\partial u_i}{\partial x_i} = 0 \tag{4}$$

$$\rho u_i \frac{\partial u_j}{\partial x_i} = -\frac{\partial P}{\partial x_j} + \frac{\partial}{\partial x_i}\left[\mu\left(\frac{\partial u_i}{\partial x_j} + \frac{\partial u_j}{\partial x_i}\right) - \rho\overline{u_i' u_j'}\right] \tag{5}$$

$$\rho C_P u_i \frac{\partial T}{\partial x_i} = \frac{\partial}{\partial x_i}\left[\lambda\frac{\partial T}{\partial x_i} - \rho\overline{u_i' T'}\right] \tag{6}$$

$$-\rho\overline{u_i'u_j'} = \mu_t\left(\frac{\partial u_i}{\partial x_j}+\frac{\partial u_j}{\partial x_i}\right)-\frac{2}{3}\delta_{ij}\rho k \quad (7)$$

where, P is pressure; U is velocity of the fluid at the inlet, $U= u+ u'$; u is the mean component of velocity; u' is fluctuating component of velocity; i and j are tensor notations. δ denotes Kronecker delta. In tensor form of Reynolds averaged Navier Stokes equation:

δ=1, if i=j;

δ=0, if $i\neq j$;

Compression work and the viscous dissipation are assumed to be negligible in the conservation of energy equation (7). In the conservation of momentum equation (5) the relative velocity is determined by expressions proposed by Manninen et al. [19] while drag function is calculated by relation given by Schiller and Naumann [21].

2.4 Turbulence modelling

For implementation of governing equations in the case of turbulent flows, experimental or approximate models are essential to take into account the turbulence phenomenon. According to Sagot et al. [22] and Menter [23], it has been suggested to use k-ω SST turbulence model for confined slot jet impingement. The k-ω SST turbulence model presents two equations, one is the turbulent kinetic energy and the other one is the specific dissipation rate. The two equations can be stated as,

$$\nabla\left(\rho_m\vec{V}_m k\right) = \nabla\left(\left(\mu+\frac{\mu_t}{\sigma_k}\right)\nabla k\right)+G_k-Y_k \quad (8)$$

$$\nabla\left(\rho_m\vec{V}_m \omega\right) == \nabla\left(\left(\mu+\frac{\mu_t}{\sigma_\omega}\right)\nabla k\right)+G_\omega-Y_\omega+D_\omega \quad (9)$$

G_k stands for the production of the turbulent kinetic energy k, for mean velocity gradients and G_ω stands for the production of the specific dissipation rate ω. Y_k and Y_ω are the dissipation term of k and ω due to turbulence. D_ω signifies cross-diffusion term.

2.5 Boundary conditions

To calculate dynamic viscosity of the Cu-water nanofluid, Brinkman model has been coded in User-Defined Functions (UDF) of ANSYS Fluent. The coupled nonlinear differential equations with the boundary conditions are resolved using the finite volume method. The pressure based solver is utilized for the numerical calculations. The second-order upwind interpolation scheme is solved for the momentum equations and energy equations. The solution is considered to converge when the normalized residual reaches below 10^{-9} for the energy equation and below 10^{-6} for all other variables. Energy equation is needed to ensure global heat balance so it is kept lower than other values.

The nanofluid jet is entered into the flow domain through nozzle with uniform inlet velocity U having a temperature T_J equal to 298 K. Pressure outlet boundary conditions (Table 2) are applied to both right and left sides. At bottom, an isothermal plate is moving in rightward direction with normalized velocity V_P, maintained at a temperature T_H of 348 K. The top surface is considered as adiabatic (Fig. 1(a)).

Table 2 Boundary conditions

Inlet nozzle	Bottom isothermal plate	Right side outlet	Left side outlet
298 K and velocity U	348 K and normalized velocity V_P	Pressure outlet	Pressure outlet

3. Results and Discussion

3.1 Validation

Fig. 2(a) and 2(b) shows the validation results of Nusselt number in contrast to previous experimental data to corroborate k-ω SST turbulence model and mixture model respectively in the present study. For the authentication of k-ω SST turbulence model for turbulence computation in the present study, validation is conducted with stationary impingement plate as experimental results [24,25] are accessible. The jets have uniform inlet velocity corresponding to Reynolds number equal to 11 000 and get impinged on a hot isothermal plate set at a temperature of 338 K. The inlet jet temperature is 373 K and geometric ratio H/W of the flow domain is equal to 6. Comparison is made with two experimental data of Cadek [24] and Gordon and Akfirat [25] and numerical result of Shariff and Banerjee [5] to show the simulated result of local Nusselt number along the impingement plate. The value of local Nusselt number in impingement region is over-predicted using k-ε turbulence model adopted by Shariff and Banerjee [5] and Manca et al. [7]. However in present study, k-ω SST turbulence model predicts closer value of the Nusselt number to the experimental data in impingement region. The k-ω SST model is an amalgamation of the k-ω model near fluid-wall interaction and k-ε model in bulk fluid region.

Fig. 2(b) shows the validation results of mixture model in terms of average Nusselt number. Mixture model is used for the modeling of Cu-water nanofluid. The present model is validated with experimented data of Wen and Ding [11] and numerical result of Lotfi et al. [26] and it shows the same trends of profile. The numerical results differ from experimental results by a little at low Reynolds number but the difference starts to diminish as Reynolds number is increased.

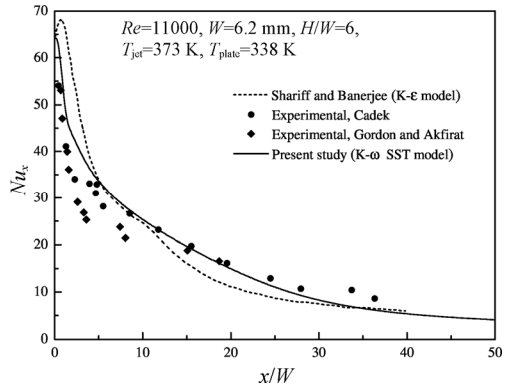

Fig. 2(a) Schematic validation of local Nusselt number

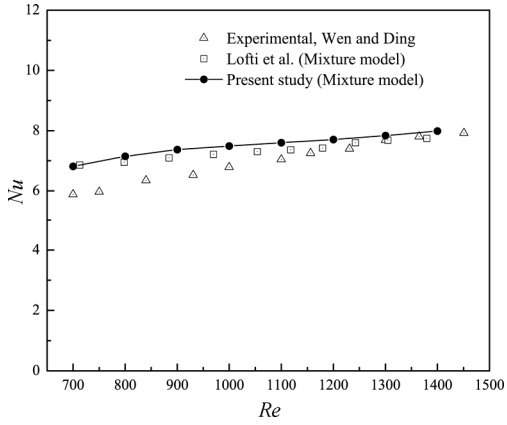

Fig. 2(b) Schematic validation of average Nusselt number

3.2 Flow field and temperature contours

Figs. 3 and 5 demonstrate the stream function contours for domain size H/W = 8 with five different moving plate velocities (V_P = 0, 0.25 0.5, 0.75 and 1) and varying nanoparticles volume concentration (φ = 0% and 5%) and Reynolds number (30 000 and 20 000) whereas Figs. 4 and 6 explain the isotherm contours for the same range. As the plate velocity is increased, substantial evolution is shown in streamline and thermal contour fields. At V_P=0, when plate is immobile, the primary vortices are produced in counter clockwise direction on right side of the jet stream and clockwise direction on the left side. This kind of vortex formation is occurred due to confinement of the flow by upper and lower boundaries and entrainment of jet flow velocity. Unlike fixed plate flow fields, discrete vortex is formed on left side of the plate near stagnation region when certain velocity is imparted to the isothermal plate. Since the relative velocity between fluid and plate increases on the left side, extra drag force is generated on respective side which results in formation of secondary drag near to the stagnation area. A significant change in mixing of jet flow is occurred while jet to jet velocity ratio increases from V_P=0 to V_P=1. The position and size of secondary vortices change drastically when nanoparticles content is increased. This result in the heat transfer rate is enhanced. It can be observed that the symmetry of flow field is disturbed and get distorted when plate gains some velocity. Because of additional vortex formation on left side near jet inlet, the flow is prevented from mixing into bulk fluid due to that convection effect is reduced considerably near that area. It is noted that moving plate velocity and jet flow velocity on downstream (right part of flow domain) are concurrent while countercurrent in upstream (left part of flow domain) followed by

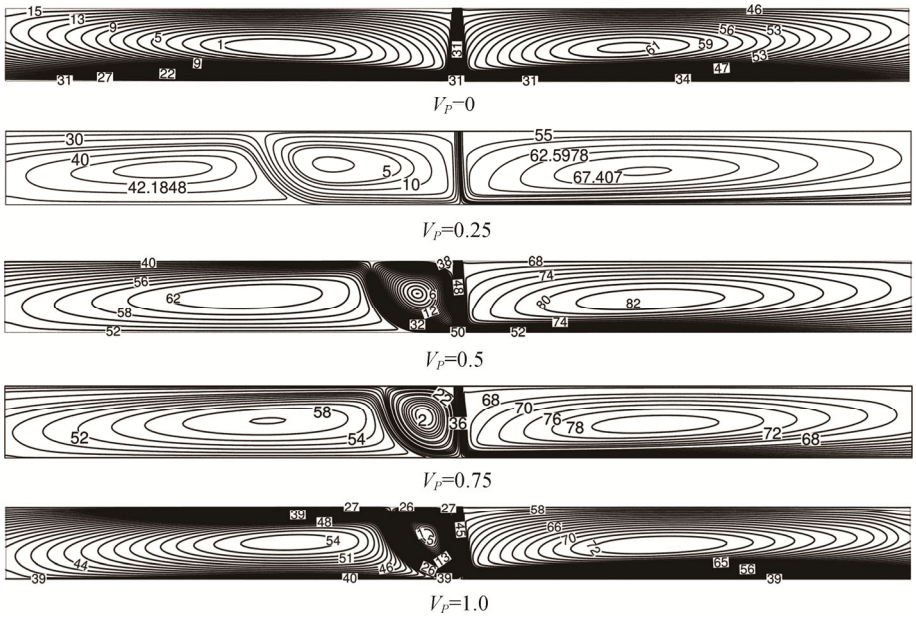

Fig. 3 Stream function contours for H/W=8, φ=0% and Re= 30 000

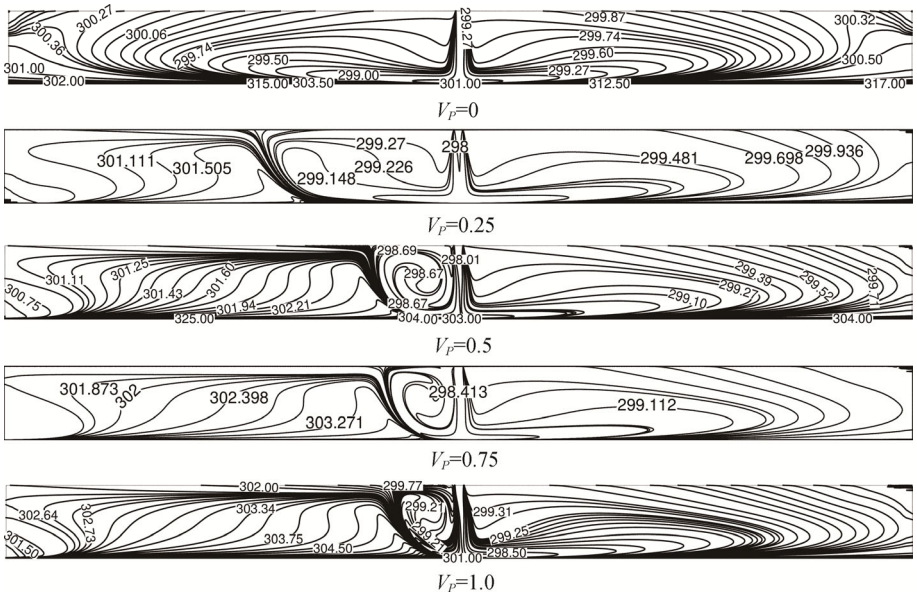

Fig. 4 Temperature contoursfor H/W=8, φ=0% and Re=30000

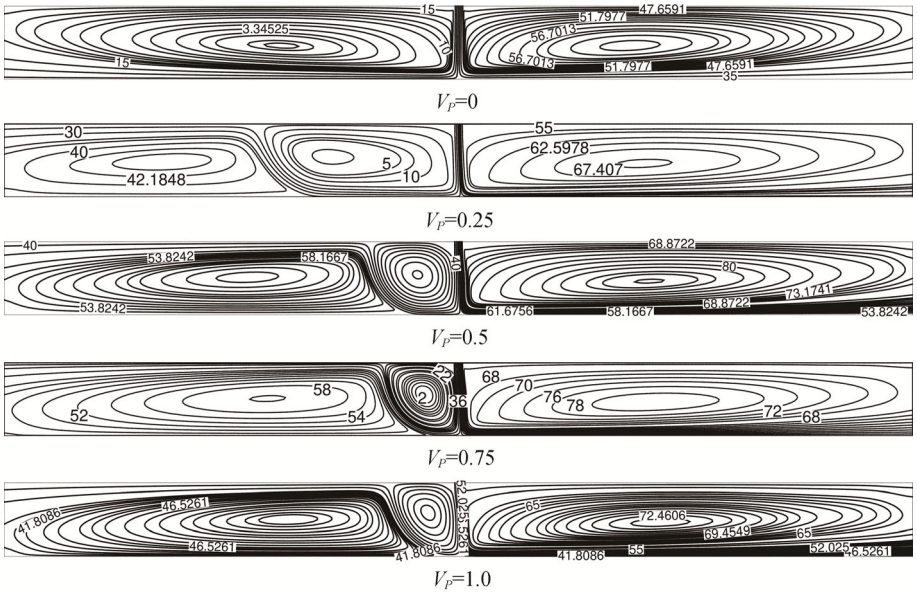

Fig. 5 Stream function contours for H/W=8, φ=5% and Re= 20 000

secondary vortices. As a consequence, fluid flow velocity is augmented in downstream and drops in upstream. As a result of the convection effect, temperature of nanofluid is enlarged on upstream side and lowered on the downstream side.

3.3 Local Nusselt number plot

3.3.1 Effect of the moving plate velocity

Figs. 7 and 8 showed the local Nusselt number plot of the isothermal plate with different cases such as for two geometric ratio H/W=6 and 8, nanoparticles volume concentration, φ = 0% and 5% with five different moving plate velocities (V_P= 0, 0.25, 0.5, 0.75 and 1) and varying Reynolds number (20 000 and 30 000) respectively. The local Nusselt number is calculated for the hot plate according to following relation:

$$Nu(x) = -\frac{W\left(\frac{\partial T}{\partial y}\right)_{y=0}}{T_H - T_J} \tag{10}$$

It is observed from Figs. 7 and 8 that the local Nusselt number profile is symmetrical in nature when the plate is stationary. As the plate moves to rightwards direction,

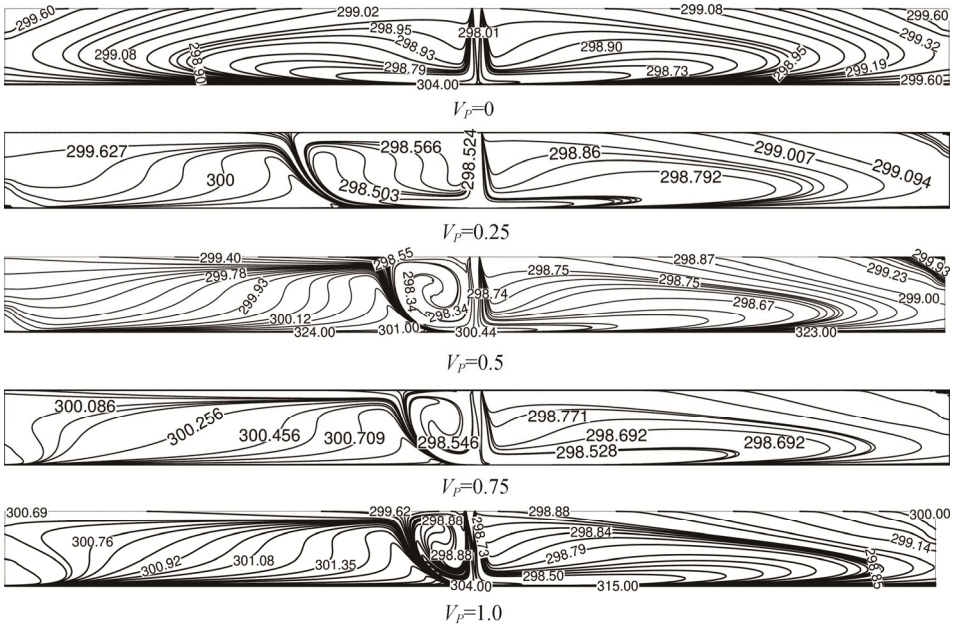

Fig. 6 Temperature contours for H/W=8, φ=5% and Re=20000

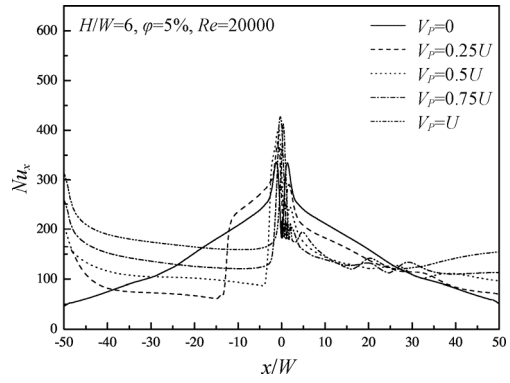

Fig. 7 Local Nusselt number for φ=5%, Re=20000 and H/W=6

heat transfer enhances on the right side whereas on the left side, heat transfer rate decreases at lower plate velocities. Huang et al. [27] found out similar kind of performance in their study. So it can be established that local Nusselt number is improved on the right side of the plate as the motion of the fluid flow is towards right-side the same as that of motion of plate. However, the motion of jet stream is opposed on the left side due to motion of the plate which is the cause of subsequent decrement in flow rate which in turn results in reduction of convective heat transfer rate. Peak value of local Nusselt number plot is found maximum when plate is imparted with velocity equal to that of jet. Furthermore, the peak value of local Nusselt number plots is augmented and shifted towards right side of the plate as the plate velocity is increased. Some disturbance which occurred at the right side of the plate can be explained by discontinuity between the velocity of moving plate and impinging jet.

3.3.2 Effect of Reynolds number

Fig. 8 (a-d) shows the difference in local Nusselt number distribution on effect of the Reynolds number (Re=20 000 and 30 000). From Figs. 8 and 9 it can be noticed that local Nusselt number curves are alike for a particular moving plate velocity. Moreover for a particular moving plate velocity, average Nusselt number and the peak value of the local Nusselt number profile is raised as the Reynolds number is increased. It is also concluded that due to rise in Reynolds number, the local Nusselt number is also improved for a particular H/W ratio.

3.3.4 Effect of H/W ratio

Figs. 7 and 8(c) show the effects of changing the separation between the slot and the impingement plate (H/W ratio equal to 6 and 8). Nevertheless, it does not show any significant change in local Nusselt number plot or average Nusselt number with changing geometric ratio (H/W) from 6 to 8.

3.3.5 Effect of volume concentration

The effect of nanoparticles concentration can be detected from Fig. 9 which demonstrates the effect of increasing nanoparticles volume concentration (φ=0%, 3%, and 5%) at a fixed Reynolds number of 20 000 and H/W ratio equal to 8. In this case, if the isothermal plate is kept stationary, then increment of 16% and 29% at φ=3% and 5% respectively is obtained in the value of average Nusselt number. Further, if the plate is moving at a velocity equal to jet velocity, then increment of 17% and

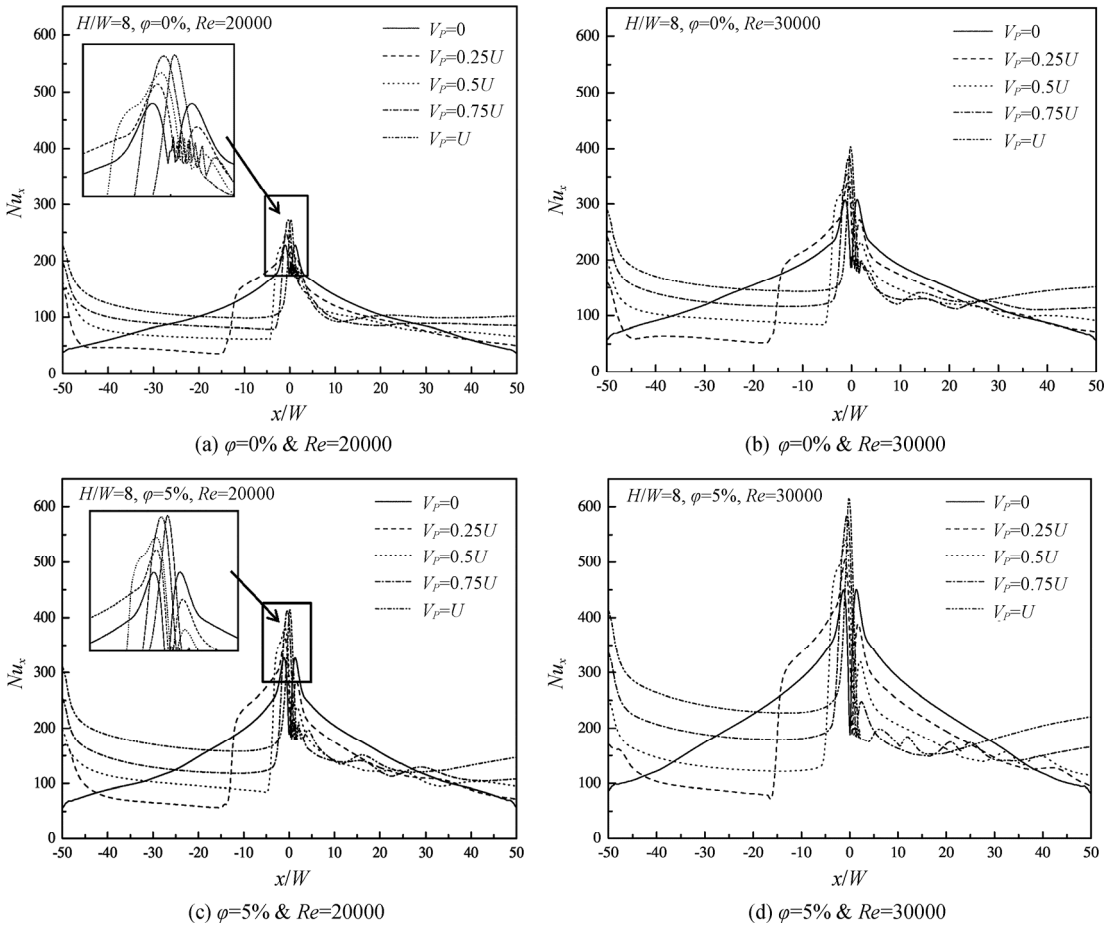

(a) φ=0% & Re=20000 (b) φ=0% & Re=30000

(c) φ=5% & Re=20000 (d) φ=5% & Re=30000

Fig. 8 Local Nusselt number plot for H/W= 8

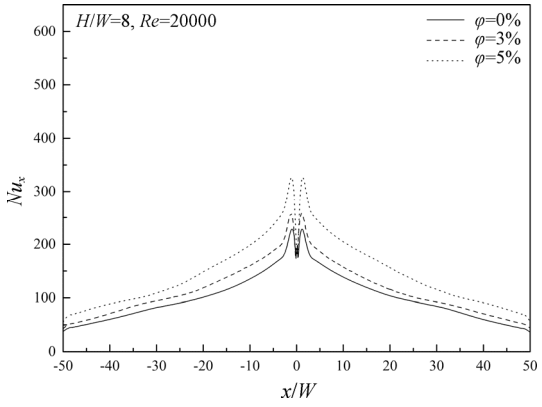

Fig. 9 Local Nusselt number plots at different nanoparticles volume concentration for stationary plate

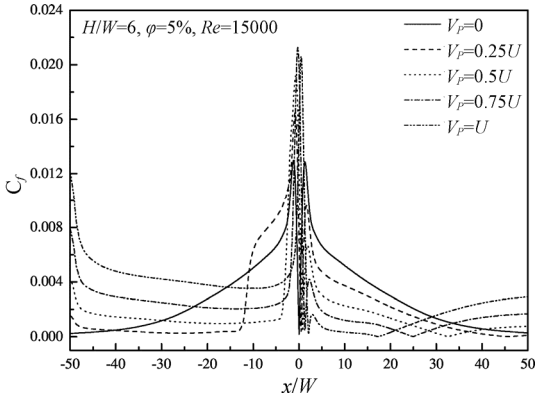

Fig. 10 Local skin friction coefficient for φ=5%, Re = 15000 and H/W=6

31% at φ=3% and 5% is obtained in the value of average Nusselt number. It is observed that increasing nanoparticles concentration increases fluid bulk temperature which elevates heat transfer rate of mixture.

3.4 Local skin-friction coefficient plot

Figs. 10 and 11 demonstrate the local skin-friction coefficient for H/W =6 and 8, φ=0% and 5% and Re=15 000 and 25 000, respectively.

The local skin-friction coefficient is calculated for the hot plate as:

$$c_f(x) = \frac{\mu\left(\frac{\partial u}{\partial y}\right)_{y=0}}{\rho U^2/2} \tag{11}$$

The peak value of the local skin-friction coefficient plot is elevated with increasing plate velocity for a particular Reynolds number, thus achieving a maximum value at

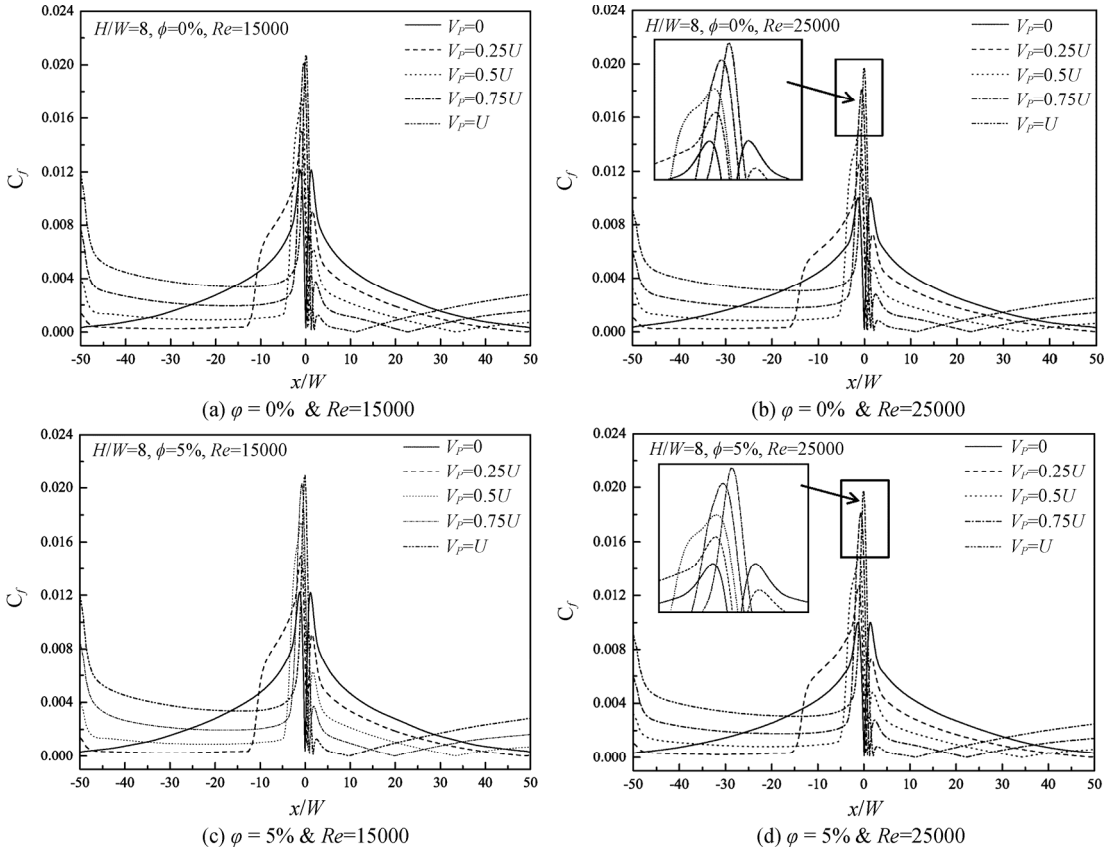

(a) φ = 0% & *Re*=15000 (b) φ = 0% & *Re*=25000

(c) φ = 5% & *Re*=15000 (d) φ = 5% & *Re*=25000

Fig. 11 Local skin friction coefficient plot for *H/W*=8

plate velocity that is equal to the jet inlet velocity. However, peak point of the local skin-friction coefficient plot is depressed with growing Reynolds number if plate velocity is kept fixed. In the case of moving plate, the profile on the left hand side is flattened since the direction of plate velocity is opposite to that of fluid flow velocity which results in greater friction between plate and fluid which further causes generation of secondary vortex near the impingement region. After reaching a maximum value at stagnation point, wall shear stress decreases as well as local skin-friction coefficient drops.

3.5 Effect of plate velocity, Reynolds number and nanoparticles concentration on average Nusselt number

Figs. 12 and 13 exhibit the evolution in average Nusselt number with changing plate velocities from 0 to 1 for different Reynolds numbers (15 000 ≤ *Re* ≤ 30 000). The average Nusselt number is computed by integrating *Nu*(*x*) over the hot plate length:

$$\overline{Nu} = \int_0^{\mathrm{L}} \frac{Nu(x)\mathrm{d}x}{\mathrm{L}} \tag{12}$$

For a particular Reynolds number, the value of average Nusselt number initially decreases with rising plate speed near V_p=0.5; then after crossing that, it rises quickly. On the other hand as the Reynolds number is augmented, heat transfer is improved. The results reveal that the dispersion of nanoparticles produces significant augmentation in the heat transfer rate. Table 3 represents percentage change in average Nusselt number for various plate velocities with respect to stationary plate at a particular Reynolds number at φ=5%. The value of average Nusselt number is minimum at V_p=0.5. Table 4 represents percentage change average Nusselt number for nanoparticles concentration changes from φ = 5% to φ = 0% at fixed Reynolds number and *H*/*W*= 8.

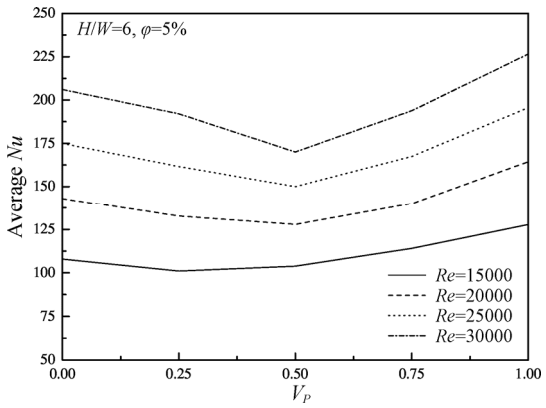

Fig. 12 Average Nusselt number for *H/W*= 6 and φ=5%

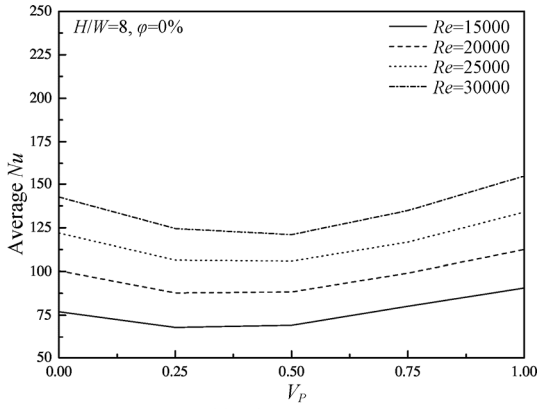

(a) H/W=8 & φ=0%

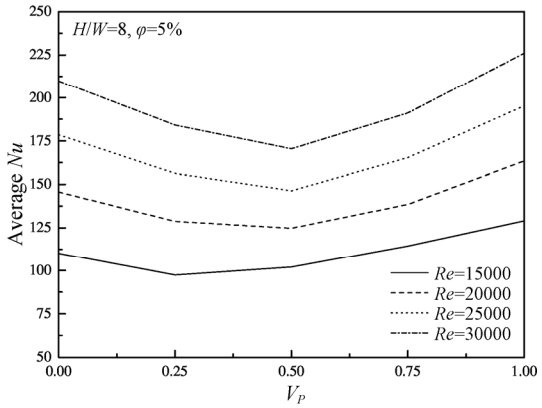

(b) H/W=8 & φ=5%

Fig. 13 Average Nusselt number for H/W=8 and φ=0% and 5%

Table 3 Percentage change in average Nusselt number for various plate velocities with respect to stationary plate at particular Reynolds number at H/W=8 and φ = 5%

V_P	0	0.25	0.5	0.75	1.0
% change at Re =30 000	0	−12.23	−18.74	8.89	7.72
% change at Re = 25 000	0	−12.41	−18.19	7.33	9.39
% change at Re = 20 000	0	−11.7	−14.35	4.92	12.27
% change at Re = 15 000	0	−11.56	−7.35	3.86	17.11

Table 4 Percentage change in average Nusselt number for nanoparticles concentration changes from φ=5% to φ=0% at H/W=8

V_P	Re= 20 000	Re= 25 000	Re= 30 000
0	0.297	0.303	0.307
0.25	0.338	0.347	0.351
0.5	0.287	0.294	0.309
0.75	0.292	0.302	0.304
1.0	0.316	0.315	0.317

3.6 Correlation of average Nusselt number

The Nusselt number of impingement jet can be interrelated to many factors such as geometric ratio (H/W), fluid properties and Reynolds number [28]. However, Martin [29] has studied impinging jet on a moving plate and found out that the main variable of the heat transfer rate as well as the flow field is the plate velocity (V_P). Since average Nusselt number has substantial implication on heat transfer in this article, average Nusselt number correlations are derived with respect to plate velocity and Reynolds number as below:

$$\overline{Nu} = 0.077\left(1-0.7534V_P+0.85V_P^2\right)Re^{0.768} \quad (13)$$

$$\overline{Nu} = 0.125Re^{0.76}Pr^{0.34}\left(1+\phi\right)^{0.58} \quad (14)$$

These correlations are considered with ±5% error.

3.7 Effect of plate velocity, Reynolds number, nanoparticles concentration and H/W ratio on average skin-friction coefficient

Figs. 14 and 15 demonstrate the average skin-friction coefficient for different Reynolds numbers and H/W ratios. The average skin friction coefficient is computed by integrating $C_f(x)$ over the hot plate length:

$$C_f = \int_0^{\mathrm{L}} \frac{c_f(x)\mathrm{d}x}{\mathrm{L}} \quad (15)$$

It is demonstrated that near V_p=0.5 middle point, the average skin friction coefficient initially decreases with plate speed. And then the value is augmented quickly with plate speed like average Nusselt number. The results also illustrate that the average skin-friction coefficient is reduced as Reynolds numbers and volume fraction is increased. However, the average skin-friction coefficient value is unchanged with rising of H/W ratios.

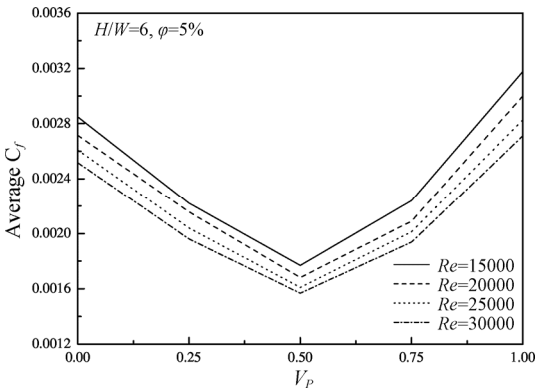

Fig. 14 Average skin friction coefficient for H/W=6 and φ=5%

4. Conclusion

Numerical investigation of flow and heat transfer process is carried out for a two-dimensional confined slot jet comprised of Cu-water nanofluid impinging on a hot moving isothermal plate. The effect of various parameters such as plate velocity, Reynolds number, nanoparticles volume concentration and geometric ratio of the flow domain on heat transfer behaviour of nanofluid jet is enquired.

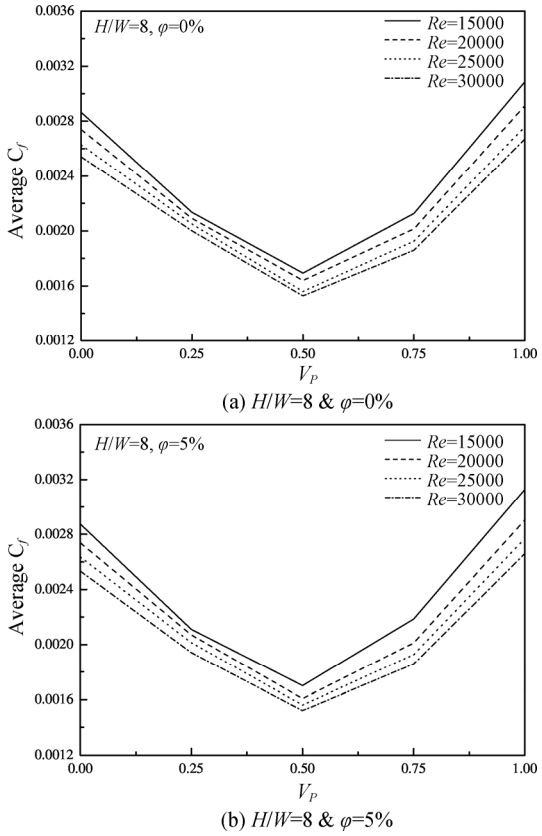

Fig. 15 Average skin friction coefficient for H/W=8 and φ=0% and 5%

Increasing nanoparticles concentration, fluid bulk temperature increases which elevate heat transfer rate of mixture. A maximum increase of 17% and 31% at nanoparticles volume concentration of 3% and 5% respectively is obtained in the value of average Nusselt number as compared to base fluid at H/W ratio of 8 and Reynolds number equal to 20 000. As the present study, increasing H/W ratio does not have appreciable effect on heat transfer. It is also proved that increasing Reynolds number increases heat transfer rate. The heat transfer mechanism and flow pattern are significantly affected due to the motion of bottom plate. The fluid flow and convective heat transfer actions are governed by impinging effect of the nanofluid jet when the plate velocity is low. As the plate velocity is increased, the overall flow field and thermal characteristics are controlled by plate motion due to dominance of shear flow. Analysis of contour plots also reveals distortion of isotherms and flow pattern and they get asymmetrical on the left side of the plate. The impinging action of jet on the target surface causes lessening of hydro-dynamic and thermal boundary layer thickness when the plate is stationary or moved with small velocities. This results in very high value of local Nusselt number and skin friction coefficient near stagnation or impingement region as compared to farther parts of the plate. These peak values are reduced due to generation of shear flow parallel to the surface when the plate is imparted with higher velocities. The average Nusselt number is reached at the lowest value near V_P = 0.5, then augments rapidly as velocity is further increased. If Reynolds number, H/W ratio and nanoparticles volume concentration are kept fixed, then there is initial decrement in the average Nusselt number which then rises quickly as plate velocity is increased. In contrast, with increase of Reynolds number and nanoparticles concentration, the average Nusselt Number rises whereas average skin friction coefficient is reduced for stationary plate.

References

[1] Choi S.U.S., Eastman J.A., Enhancing thermal conductivity of fluids with nanoparticles. American Society of Mechanical Engineers. Fluids Engineering Division (Publication) FED, 1995, pp. 99–105.

[2] Masuda H., Ebata A., Teramae K., Hishinuma N., Alteration of thermal conductivity and viscosity of liquid by dispersing ultra-fine particles (Dispersion of γ - Al_2O_3, SiO_2, and TiO_2 Ultra-fine particles.). NetsuBussei, 1993, 7(4): 227–233. (in Japanese)

[3] Kilic M., Calısır T., Baskaya S., Experimental and numerical study of heat transfer from a heated flat plate in a rectangular channel with an impinging jet. Journal of the Brazilian Society of Mechanical Sciences and Engineering, 2017, 39(1): 329–344.

[4] Kilic M., Calısır T., Baskaya S., Experimental and numerical investigation of vortex promoter effects on heat transfer from heated electronic components in a rectangular channel with an impinging jet. Heat Transfer Research, 2017, 48(5): 435–463.

[5] Sharif M.A.R., Banerjee A., Numerical analysis of heat transfer due to confined slot-jet impingement on a moving plate. Applied Thermal Engineering, 2009, 29(2–3): 532–540.

[6] Roy G., Nguyen C.T., Lajoie P., Numerical investigation of laminar flow and heat transfer in a radial flow cooling system with the use of nanofluids. Super Lattices and Microstructures, 2004, 35(3-6): 497–511.

[7] Manca O., Mesolella P., Nardini S., Ricci D., Numerical study of a confined slot impinging jet with nanofluids. Nanoscale Research Letters, 2011, 6(1): 188.

[8] Kilic M., Muhammad A., Numerical investigation of combined effect of nanofluids and multiple impinging jets on heat transfer. Thermal Science, 2018, doi.org/10.2298/TSCI171204094K.

[9] Xuan Y.M., Li Q., Investigation on convective heat transfer and flow features of nanofluids. ASME Journal of Heat Transfer 2003, 125(2): 151–155.

[10] Li Q., Xuan Y.M.: Convective heat transfer and flow characteristics of Cu-water nanofluid. Science in China Series E: Technological Science 2002, 45(4): 408–416.

[11] Wen D., Ding Y., Experimental investigation into convective heat transfer of nanofluids at the entrance region under laminar flow conditions. International Journal of Heat and Mass Transfer, 2004, 47: 5181–5188.

[12] Rashidi S., Akar S., Bovand M., Ellahi R., Volume of fluid model to simulate the nanofluid flow and entropy generation in a single slope solar still. Renewable Energy, 2018, 115(C): 400–410.

[13] Ellahi R., Zeesham A., Shehzad N., Sultan Z., Structural impact of Kerosene-Al2O3 nanoliquid on MHD Poiseuille flow with variable thermal conductivity: Application of cooling process. Journal of Molecular Liquids, 2018, 264: 607–615.

[14] Akbarzadeh M., Rashidi S., KarimiN., Convection of heat and thermodynamic irreversibilities in two-phase, turbulent nanofluid flows in solar heaters by corrugated absorber plates. Advanced Powder Technology, 2018, 29(9): 2243–2254.

[15] Shirvan K. M., Ellahi R., Mamourian M., Moghiman M., Effect of wavy surface characteristics on heat transfer in a wavy square cavity filled with nanofluid. International Journal of Heat and Mass Transfer, 2017, 107: 1110–1118.

[16] Ellahi R., Tariq M. H., Hassan M., Vafai K., On boundary layer magnetic flow of nano-ferroliquid under the influence of low oscillating over stretchable rotating disk. Journal of Molecular Liquids, 2017, 229: 339–345.

[17] Rajendran D.R., Ganapathy Sundaram E., Jawahar P., Experimental studies on the thermal performance of a parabolic dish solar receiver with the heat transfer fluids SiC + water nano fluid and water. Journal of Thermal Science, 2017, 26(3): 263–272.

[18] Brinkman H.C., The viscosity of concentrated suspensions and solutions. Journal of Chemical Physics, 1952, 20(4): 571–581.

[19] ANSYS Inc. ANSYS Fluent 15.0 UDF Manual, Canonsburg, PA: ANSYS Inc, 2013.

[20] Manninen M., Veikko T., Sirpa K., On the mixture model for multiphase flow. Valtion Teknillinen Tutkimuskeskus publication, 1996: 3–67.

[21] Schiller L., Naumann Z., A drag coefficient correlation. Zeitschrift des Vereins Deutscher Ingenieure, 1935, 77: 318: 51. (in German)

[22] Sagot B., Antonini G., Christgen A., Buron F., Jet impingement heat transfer on a flat plate at a constant wall temperature. International Journal of Thermal Sciences, 2008, 47(12): 1610–1619.

[23] Menter F.R., Two-equation eddy-viscosity turbulence models for engineering applications. AIAA Journal, 1994, 32(8): 1598–1605.

[24] Cadek F.F.A., Fundamental investigation of jet impingement heat transfer. Ph.D Theis. University of Cincinnati, the United States, 1968.

[25] Gordon R., Akfirat J.C., Heat transfer characteristics of impinging two-dimensional air jets. ASME Journal of Heat. Transfer, 1966, 88(1): 101–108.

[26] Lotfi R., Saboohi Y., Rashidi A.M., Numerical study of forced convective heat transfer of nanofluids: comparison of different approaches. International Journal of Heat and Mass Transfer, 2010, 37(1): 74–78.

[27] Huang P.G., Mujumdar A.S., Douglas W.J.M., Numerical prediction of fluid flow and heat transfer under a turbulent impinging slot jet with surface motion and cross flow. ASME paper, 1984, 84: WA/HT-33.

[28] Zuckerman N., Lior N., Jet impingement heat transfer: Physics, correlations, and numerical modeling. Advances in Heat Transfer, 2006, 39: 565–631.

[29] Martin H., Heat and mass transfer between impinging gas jets and solid surface. Advances in Heat Transfer, 1977, 13: 1–60.